A Numerical Study on Harnessing Powder Technology to Mechanically Improve Titanium Alloys Used in Aircraft Turbines

Khaldoon Hussein Hamzah[1], Saleh Jawad Hamza[1], Qasim Saad Abdulwahid[2]

[1]*Lecturer, Department of Materials Engineering, College of Engineering, University of Al-Qadisiyah, Iraq*
[2]*Assistant Lecturer, Department of Materials Engineering, College of Engineering, University of Al- Qadisiyah, Iraq*
Email: khaldoon.hussein@qu.edu.iq

Abstract: This research investigates the use of powder technology to improve the mechanical properties of titanium alloys, particularly for aviation turbine components. It uses advanced computational modeling and simulation methods to examine the mechanical characteristics of titanium alloys made using powder metallurgy processes like powder sintering and additive manufacturing. The study evaluates the impact of process variables, powder properties, and post-processing processes on the performance of the finished titanium alloy components. The simulation of powder in aircraft engine turbine manufacturing involves creating a model of a standard engine and adding titanium powder layers to increase its aerodynamic resistance. The model is then entered into the FSI system, where aerodynamics are studied at speeds of 200, 400, and 600 km/h. The properties of Ti–6Al–4V are then applied to the turbine structure using different thicknesses of powder. The speed of a plane impacts the air flow speed and gradients of an engine turbine, causing a force on the blades. The thickness of the powder layer affects the deformations caused by air force. Powder technology offers benefits, with the 5mm layer having the highest deformation. The stress generated by the plane's force is 3.2 GPa, while the deformation value is 0.452 m at 600 km/h.

Keywords: Titanium Alloys, Powder Metallurgy, Aerodynamics Simulation.

1. Introduction

Titanium alloys are crucial in the aerospace sector for aircraft engine design due to their strength-to-weight ratio, high-temperature resistance, and corrosion resistance. As aviation technology advances, the need for more sophisticated titanium alloys is increasing. Powder technology, specifically additive manufacturing and powder sintering, can be used to improve mechanical properties and lower production costs. This research investigates the use of powder technology to enhance the mechanical properties of titanium alloys for aviation turbines. It uses computational modeling and simulation methods to understand the interaction between powder manufacturing parameters, material properties, and mechanical performance. The goal is to create a new class of titanium alloys that are stronger, lighter, and more affordable. This research will contribute to the aerospace industry's push for more effective and environmentally friendly aircraft turbine technology.

(Telang et al., 2021) [1] The use of magnesium (Mg) and its alloys in orthopaedic applications, such as porous scaffolds and biodegradable bioimplants, is growing. These scaffolds are useful for tissue engineering because they are biocompatible, bioabsorbable, and bioactive. Bioimplants made of magnesium are more biocompatible and nontoxic than human bone. But because of its chemical and thermal instability, which may lead to corrosion and early failure in vivo, manufacturing magnesium alloys is difficult. This study focuses on the processing and additive manufacturing of magnesium alloy powder and paste-based degradable bioimplants, emphasizing current advancements and potential future applications. (Allavikutty et al., 2021) [2] Magnesium and magnesium-based alloys are next-generation biomaterials due to their ability to dissolve into bodily fluids without residue. They offer mechanical strength comparable to bone, bioabsorbable and bioresorbable properties, and deterioration regulation. Traditional production methods struggle to replicate their intricate form, but additive manufacturing can be used to create complex components. Understanding the link between microstructure and properties is crucial for producing magnesium alloys. (Kim et al., 2020) [3] Investigated the biological properties of 3D-printed titanium alloys for dental applications. It compares the biological activities of machine-cut and 3D-printed specimens using DLMS 3D printing parameters. The study used medical-grade Ti-6Al-4V powders, adjusted laser spacings, and post-surface treatment conditions. The initial cell adhesion of the optimized DLMS 3D-printed specimen was compared with that of the machine-cut specimen. Results showed that laser spacings of 30-40 m had less interior flaws, greater three-point flexural strength, and elastic modulus. Sandblasted specimens showed decreased surface roughness and better hydrophilicity, making them ideal for biological investigation. The study suggests the potential use of 3D printing technology for various dental applications.

(Yang et al., 2020) [4] examined the impact of unit cell size on Schwartz diamond graded porous structures (SDGPSs) for bone implant applications. Results show that SDGPSs can be successfully printed using laser powder bed fusion (LPBF) with a range of 3.5 mm to 5.5 mm. The study also found that as unit cell size increases, the mechanical characteristics of LPBF-printed SDGPSs improve, and the energy absorption capacity decreases. (Alshammari et al., 2020) [5] Explored the production of Ti-x Cu/Mn alloys using powder metallurgy. The alloys undergo one-step forging in the "+" field, with microstructures, mechanical characteristics, and impact. The alloys show comparable ultimate tensile strength and Vickers hardness to forged Ti-Cu/Mn alloys, even at lower forging temperatures. (Quazi et al., 2020) [6] reviewed laser welding of titanium alloys with other materials, highlighting the impact of processing factors on metallurgical characteristics. It discusses methods like laser offsetting, split beam, welding-brazing, hybrid welding, and material modifications. The study also explores the formation and distribution of intermetallic phases, material flow, and flaw development. The goal is to highlight the advantages and popularity of laser welding Ti alloys in academia, enabling better application in business and further research.

(Smythe et al., 2020) [7] Wire deposition additive manufacturing (AM) has increased research and development spending in the last 20 years, particularly for high-value materials like alloyed titanium. However, waste from powder-based AM is a significant issue. The ConformTM continuous extrusion method combines waste titanium alloy feedstocks, allowing wire samples to be cold-drawn down to 40%. This technology could contribute to the circular economy and environmentally friendly supply chains in the aerospace industry. (Davis et al., 2019) [8] A preliminary investigation examined the use of high deposition rate WAAM to print dual-alloy microstructures. Samples were constructed using Ti and Ti-6Al-4V feed wires. The dual alloy composite material showed a twofold inflection yield behavior and yield strength in the middle of the two alloys. The refined-grain structure suggests composition gradients may disturb epitaxial columnar development in WAAM deposits. (Subbarao and Chakraborty, 2018) [9] Gas turbine technology is rapidly expanding due to declining traditional fuel supplies. Experimental work on better materials, such as steel, titanium, and nickel alloys, is being

conducted to improve the lifespan and application range of gas turbines. Microscopic investigations, hardness, and surface roughness measurements are used to analyze the grain structure and other properties of these alloys. The study aims to identify the right alloy for long-lasting gas turbine components, providing additional options for future electricity production. (Yap et al., 2015) [10] Selective laser melting (SLM) is a rapid prototyping, additive manufacturing, or 3D printing process that uses a high-power-density laser to melt and fuse metallic powders to create components with near-net shapes and up to 99.9% relative density. With advancements in fiber optics and laser technology, SLM can now treat various metallic materials, including copper, aluminum, and tungsten, as well as ceramic and composite materials. This review provides an overview of the material qualities produced by SLM and current research trends.

(Song et al., 2012) [11] Examined the processing parameters of selective laser melting to create denser Ti6Al4V components without post-processing. A three-dimensional model calculates the temperature distribution, revealing a significant temperature gradient from the powder bed's surface to the experimental platform. The study successfully creates Ti6Al4V components with reduced porosity and greater density at a laser power of 110 W and a scan rate of 0.2 m/s. (Murr et al., 2009) [12] Electron beam melting and selective laser melting processes are used to create basic product geometries in layers, comparing their microstructure and mechanical behavior to traditional Ti-6Al-4V products. Microstructures are characterized using optical metallography, SEM, and TEM, and their benefits and drawbacks are explored for custom biomedical components.

2. Methodology

The process of simulating the use of powder in the manufacture of aircraft engine turbines requires designing a model of a standard engine with real dimensions and adding powder layers to it of titanium to increase the ability to withstand the pressures resulting from aerodynamics.

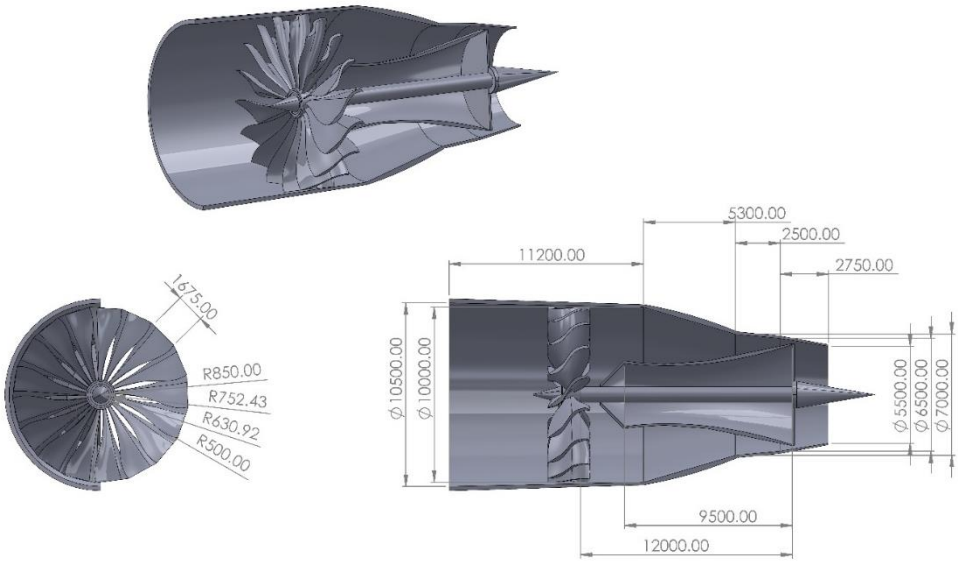

Figure 1. *Geometry simulation*

Since unstructured grids tend to work well for complicated geometries, a tetrahedron grid was employed in this investigation. In ANSYS, users just need to provide input in a single phase to generate a mesh for a solid geometry or a 3D model. In this work, a total of (2204659) cells were collected see figure (2).

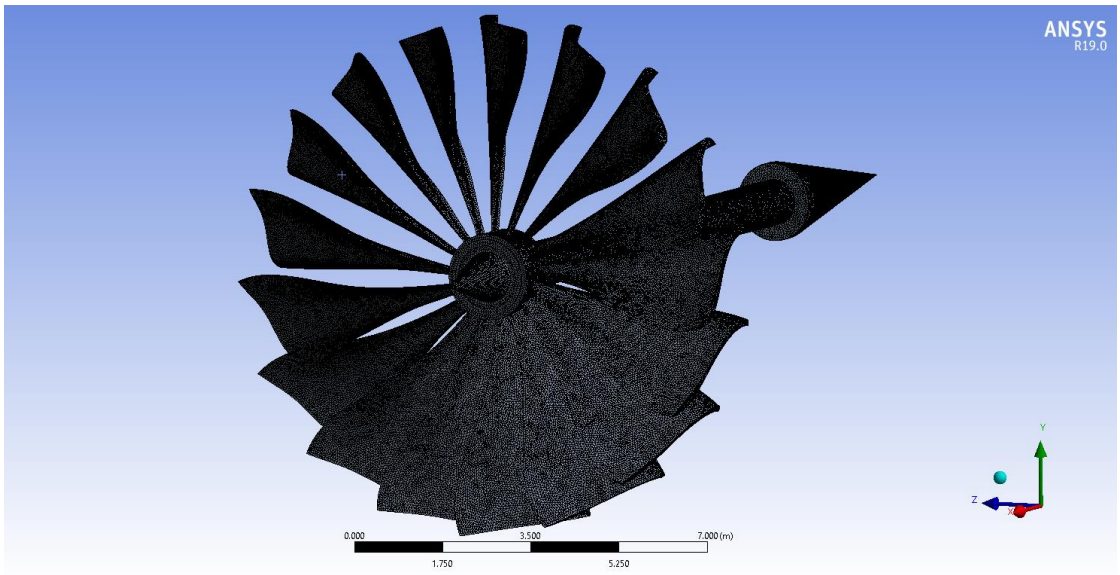

Figure 2. *Mesh generated.*

The simulation process requires the work of complex algorithms to solve the matrices contained in the domain, and therefore an accurate mesh must be made to solve the equations. Then work the reliability of the mesh for a solution to reach a stable state with the results. Because of the multiplicity of models that have been simulated, it is necessary to make more than one mesh and more than one mesh reliability. The value of the element was 2204659 when the Maximum deformation arrived at 0.754 as in Table 1.

Table 1. *Mesh independency.*

Case	Element	Node	Max deformation (m)
1	1017634	1603452	0.831
2	1516036	2312565	0.767
3	1834604	2864545	0.755
4	2204659	3262597	0.754

After the process of forming the model, it was entered into the FSI system, where the aerodynamics are dealt with by entering at speeds of 200, 400, and 600 km/h to see the amount of force exerted on the engine turbines. Then, the properties of Ti–6Al–4V that were obtained through Murr's research [12] were introduced with different thicknesses of 5mm, 10mm, and 15mm as a pouring powder on the surfaces of the turbine structure. As figure 3.

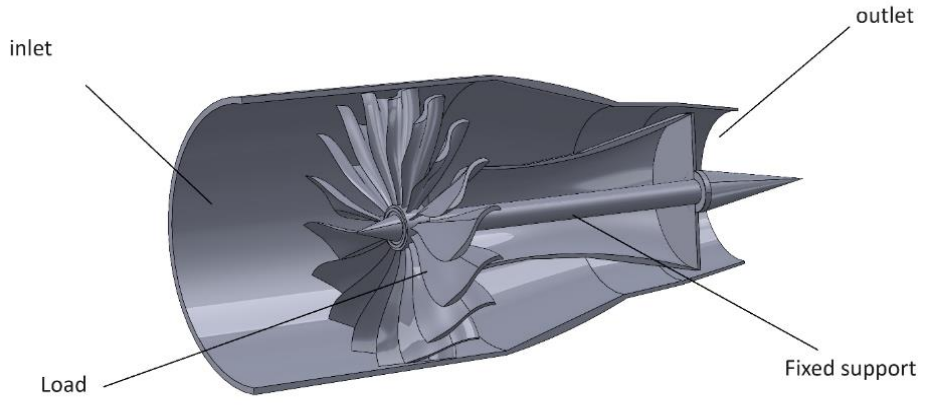

Figure 3. *Boundary condition.*

2.1 Governing Equations

2.1.1 Standard k-ϵ Model

The following transport equations are used to determine the kinetic energy of the turbulence, k, and its rate of dissipation:

$$\frac{\partial}{\partial t}(\rho k) + \frac{\partial}{\partial x_i}(\rho k u_i) = \frac{\partial}{\partial x_j}\left[\left(\mu + \frac{\mu_t}{\sigma_k}\right)\frac{\partial k}{\partial x_j}\right] + G_k + G_b - \rho\varepsilon - Y_M + S_k \quad (1)$$

and

$$\frac{\partial}{\partial t}(\rho \varepsilon) + \frac{\partial}{\partial x_i}(\rho \varepsilon u_i) = \frac{\partial}{\partial x_j}\left[\left(\mu + \frac{\mu_c}{\sigma_z}\right)\frac{\partial \varepsilon}{\partial x_j}\right] + C_{1z}\frac{\varepsilon}{k}(G_k + C_{3c}C_b) - C_{2z}\rho\frac{\varepsilon^2}{k} + S_s \quad (2)$$

G_k, which is determined in accordance with the instructions in Modeling Turbulent Production in the k-e Models, denotes the creation of turbulence kinetic energy resulting from mean velocity gradients. Effects of Buoyancy on Turbulence in the k-e Models describes how to computeG_b, which is the kinetic energy generated by buoyancy that causes turbulence. As computed in Effects of Compressibility on Turbulence in the k-e Models, $Y_M$represents the variable dilatation in compressible turbulence's contribution to the total dissipation rate. Constants include C_{1r}, C_{2r} andC_{32}. The turbulent Prandtl numbers for k and ε_r are σ_ε andσ_k, respectively. User-defined source terms S_k and $S_z$are used.

Combining k and, the turbulent (or eddy) viscosity,μ_t is calculated as follows:

$$\mu_t = \rho C_\mu \frac{k^2}{\varepsilon} \quad (3)$$

where C_μ is a constant. The model constants $C_{1\varepsilon}, C_{2\varepsilon}, C_\mu, \sigma_k$, and σ_ε have the following default values:

$$C_{1x} = 1.44, C_{2r} = 1.92, C_\mu = 0.09, \sigma_k = 1.0, \sigma_z = 1.3$$

These default values were established by studies on fundamental turbulent flows, including boundary layers, mixing layers, and jets—shear flows that are regularly encountered—as well as on decaying isotropic grid turbulence. They have been discovered to function rather well for a variety of free and wall-bounded shear flows. Although the model constants' default values are the established industry standards, you can alter them (if necessary) in the Viscous Model Dialog Box.

2.1.2 Mass Equation

The commitment to the mass hotspot for ease p in a cell is

$$m_p = -m_{pq'} \quad (4)$$

and for phase q is

$$m_q = m_{p'q'} \quad (5)$$

2.1.3 Momentum Equation

there is no energy source. For the Eulerian model, the energy source in a cell for stage p is

$$m_p\vec{u}_p = -m_{piq}\vec{u}_p \quad (6)$$

and for phase q is

$$m_q\vec{u}_q = m_{pqq}\vec{u}_p \quad (7)$$

2.1.4 Energy Equation

For every single multiphase model, the accompanying energy sources are added. The energy source in a cell for stage p is

$$H_p = -m_{p^i q^i}\left(h_q^{f^i} - h_p^{f^k}\right) \quad (8)$$

and for phase q is

$$H_q = m_{p^i q'} \left(h_q^{f^j} - h_p^{f^i} \right) \quad (9)$$

where $h_p^{f^i}$ and $h_q^{f^j}$ are the arrangement enthalpies of species i of stage p and species j of stage q, separately. The distinction between $h_p^{f'}$ and $h_q^{f^j}$ is the dormant intensity.

3. Results and discussion

In this section, all the results obtained through the simulation program for harnessing titanium powder on a jet engine turbine will be reviewed.

3.1 The effect of aircraft speed on the force acting on turbines

The impact of aircraft speed on turbine forces is crucial in aviation and aerospace engineering. Understanding how turbines interact with air at different speeds is essential for safe and effective flying. Turbines are key parts of aviation engines and are affected by various factors such as aerodynamic forces, drag, centrifugal forces, compressor efficiency, and heat load. Aerodynamic forces convert kinetic energy into mechanical work by turbine blades, while drag forces oppose the aircraft's forward motion and are affected by speed. Centrifugal forces push on turbine blades, affecting their structural integrity. Compressor efficiency is also affected by aircraft speed, affecting the compressor's performance and affecting turbine forces. Heat load changes based on an aircraft's speed, affecting the combustion process and affecting the temperature and thermal loads of turbine parts. Understanding and forecasting the effects of aircraft speed on turbine forces is essential for safe and effective aircraft operations. Engineers and researchers use computational fluid dynamics simulations, wind tunnel testing, and other analytical techniques to optimize turbine design for various flight situations. Figures 4 and 5 show the air flow speed of the engine turbine and its gradients.

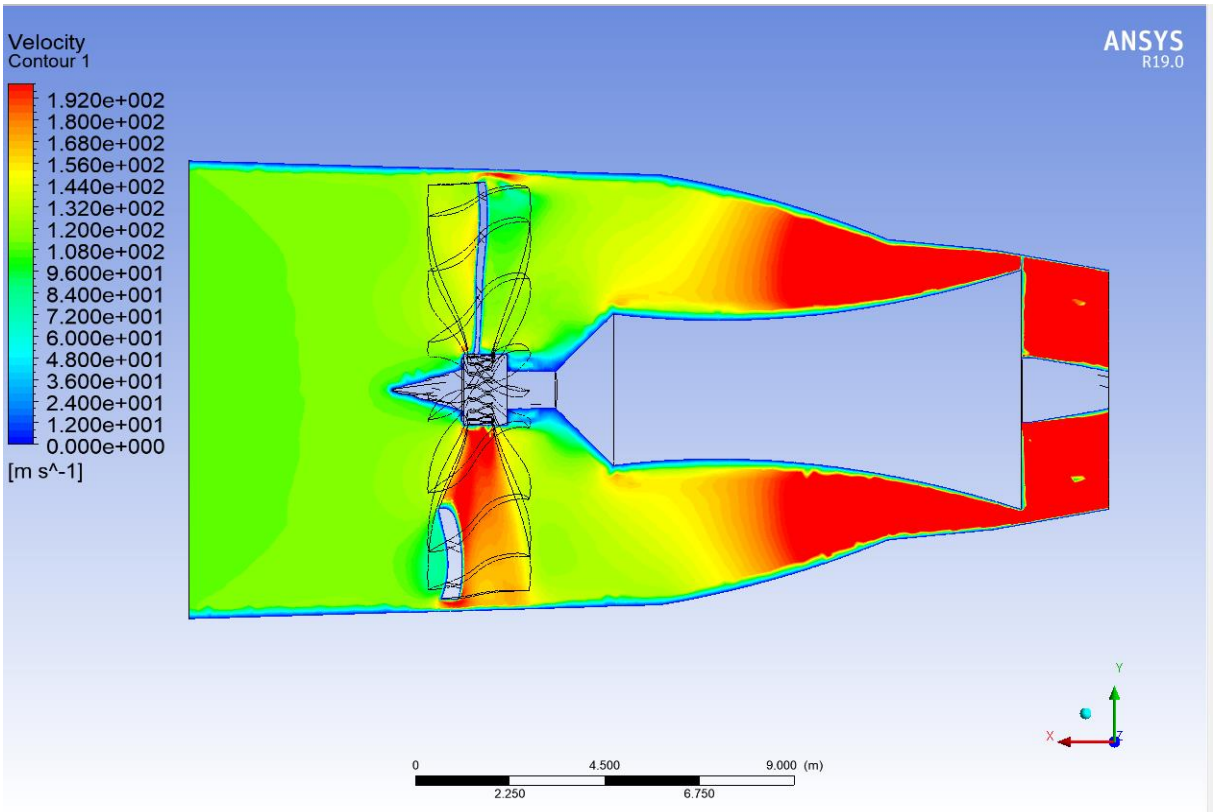

Figure 4. *Velocity contour of jet turbine.*

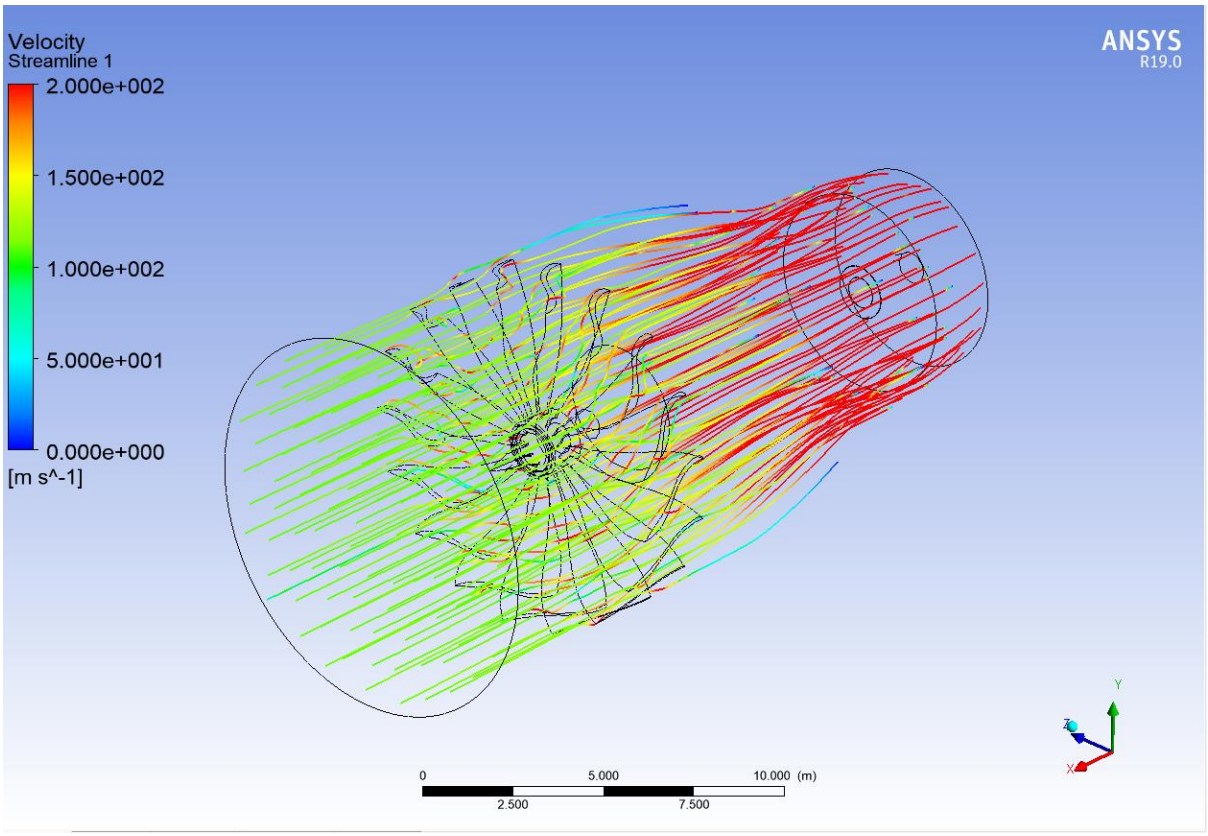

Figure 5. *Streamline of jet turbine.*

Figure 6 shows the effect of the plane's speed on the force exerted on the turbine blades. Thus, the speed of 600 kilometers per hour reached 13 mega newton's.

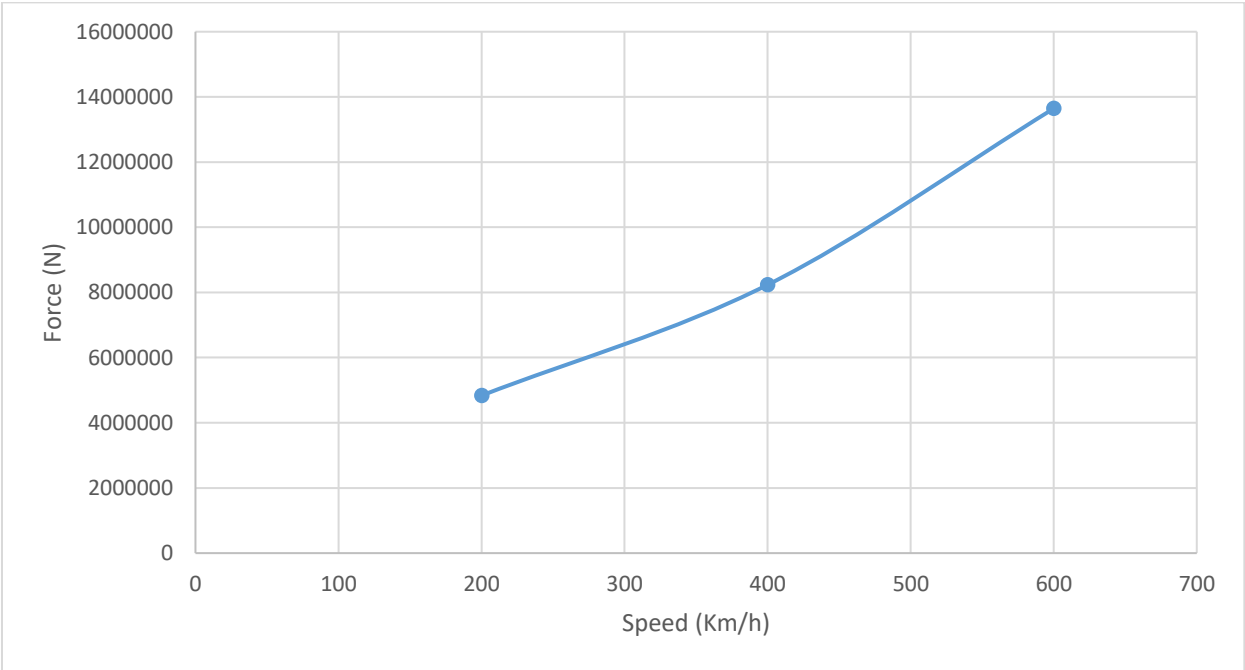

Figure 6. *Force on turbines gradient with speed of aircraft.*

3.2 Effect of Ti–6Al–4V harnessing powder layer thickness

The thickness of Ti-6Al-4V powder layer during additive manufacturing processes like selective laser melting (SLM) and electron beam melting (EBM) significantly impacts

deformation. Thinner layers provide a more regulated cooling process, potentially lowering thermal strains. Energy input must be adjusted to account for varying layer thicknesses, as thicker layers may require more energy to melt the powder, resulting in different temperature profiles and deformation. Residual stress, which maintains heat between layers, may result in larger amounts of residual stress, causing the finished portion to bend and distort. The size of the melting pool may also affect the deformation properties of the finished product. Support structures may be required based on the layer thickness, with thicker layers needing stronger support systems to avoid warping or sagging. The part's orientation on the build platform also affects deformation, with layer thickness selection affecting the ideal construction orientation. The size of the component being manufactured also influences layer thickness selection. Simulators and experiments can be useful tools for determining the ideal layer thickness for a specific application.

Figure 7 shows the effect of the thickness of the powder layer on the amount of deformations resulting from the air force passing through the turbine blades. The deformation at the 5 mm layer reached 0.73 m, while at the 10 mm thickness it was 0.44 m, while at the 15 mm thickness it was 0.27 m. This shows the benefit of using powder technology. In improving the properties of the material.

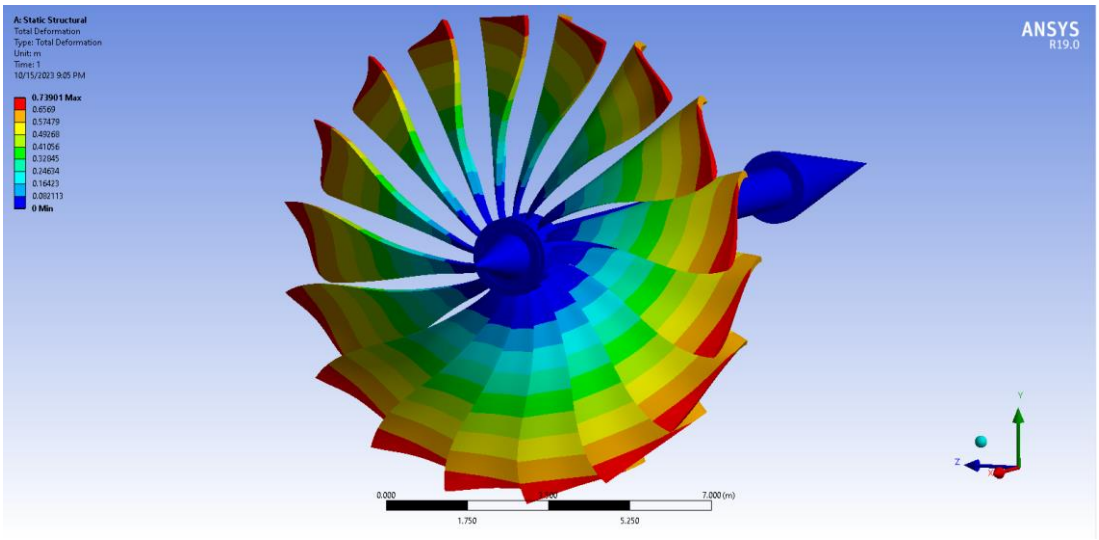

(a)

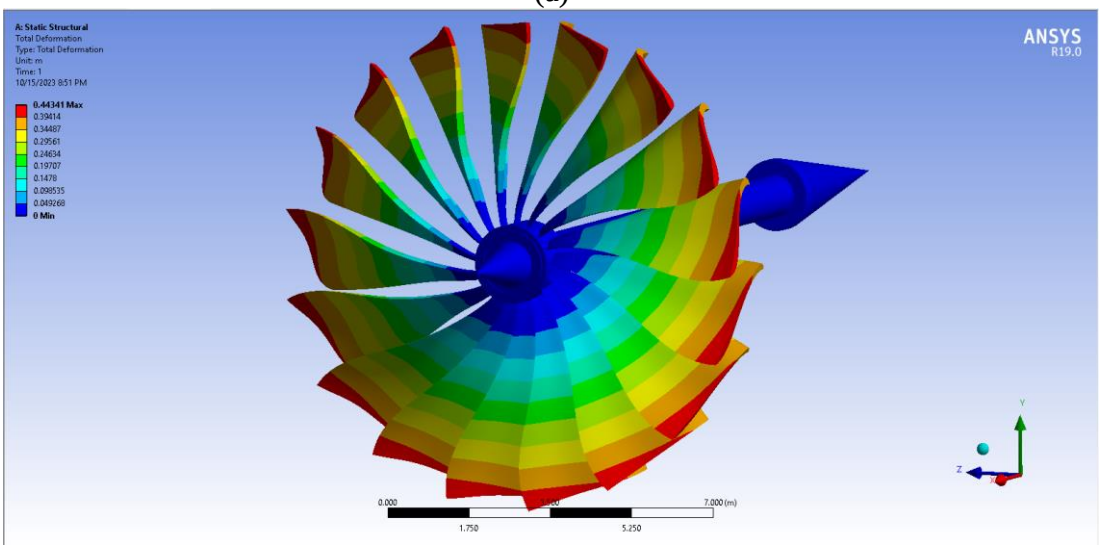

(b)

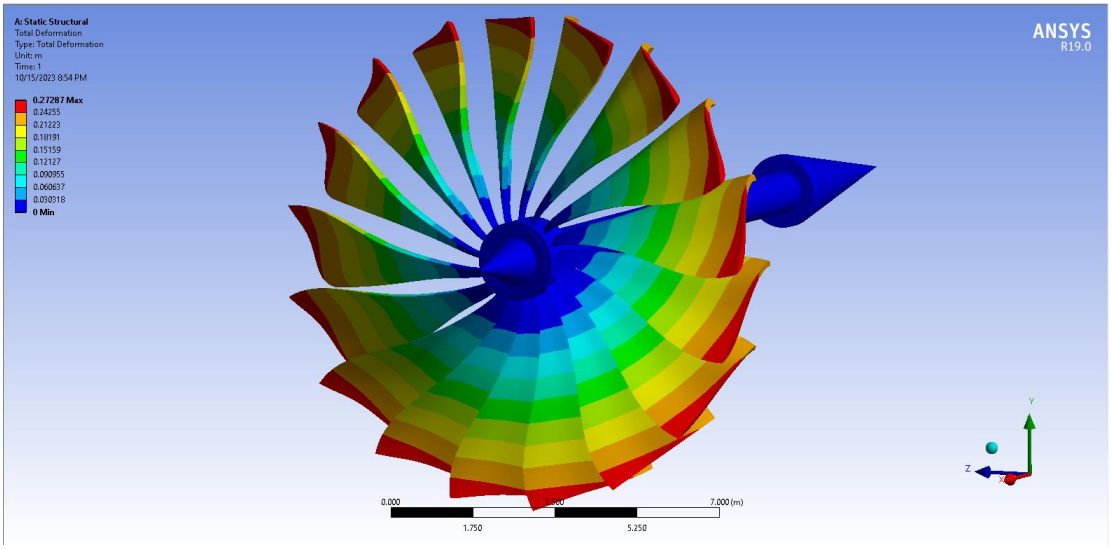

(c)

Figure 7. *Deformation contour at speed 400 Km/h and different Ti–6Al–4V harnessing powder layer thickness. (a) 5mm,(b)10mm,(c)15mm.*

Figure 8 shows the amount of stress generated because of the force applied to it, where the stress reached 3.2 GPa.

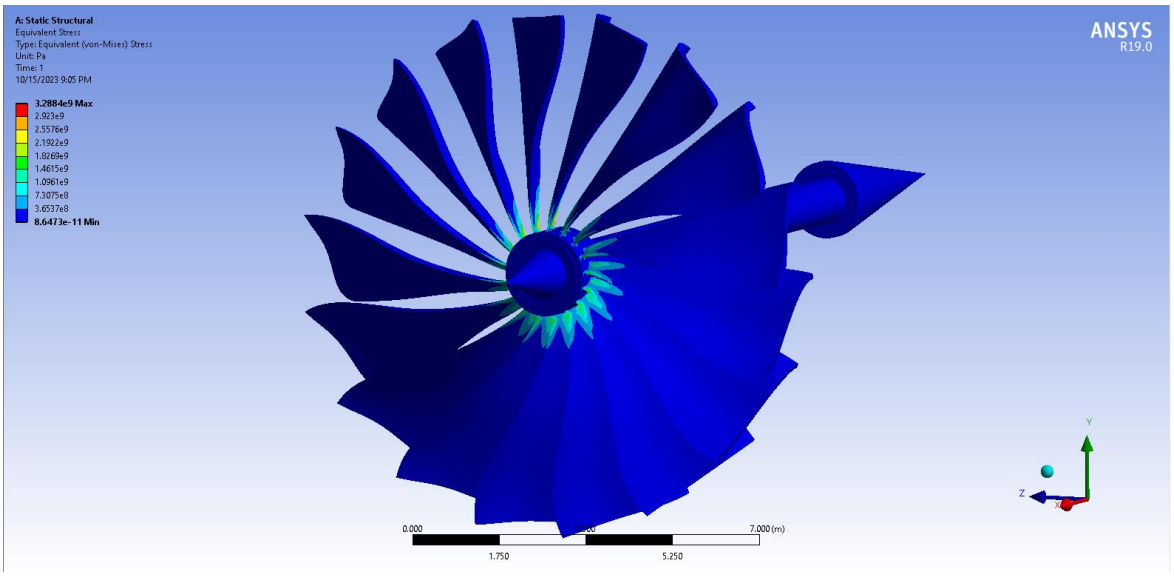

Figure 8. *Stress contour at speed 400 Km/h and different Ti–6Al–4V harnessing powder layer thickness.*

3.3 Effect of aircraft speed on Ti–6Al–4V harnessing powder

The impact of aircraft speed on Ti-6Al-4V powder harnessing is not directly related to the aircraft's speed, but rather to the additive manufacturing process. The material's resistance to dynamic stresses during high-speed flight is crucial, as it should result in components with the required mechanical toughness. Thermal effects, such as air friction, also affect the material's properties, necessitating proper heat management and thermal insulation. Aerodynamic design, particularly those produced by additive printing, is influenced by the aircraft's speed, and Ti-6Al-4V parts should be optimized for weight reduction and high-speed performance. The manufacturing process, whether using powder bed fusion or another method, should be meticulously regulated to ensure the finished components meet the required criteria.

In conclusion, the speed of an aircraft indirectly influences the design and performance of aircraft components made from Ti-6Al-4V, but not directly. Figure 9 shows the effect of the plane's speed on the formation of a greater force and thus more stress and greater deformation, as the deformation value reached 0.452 m at the speed of 600 km/h.

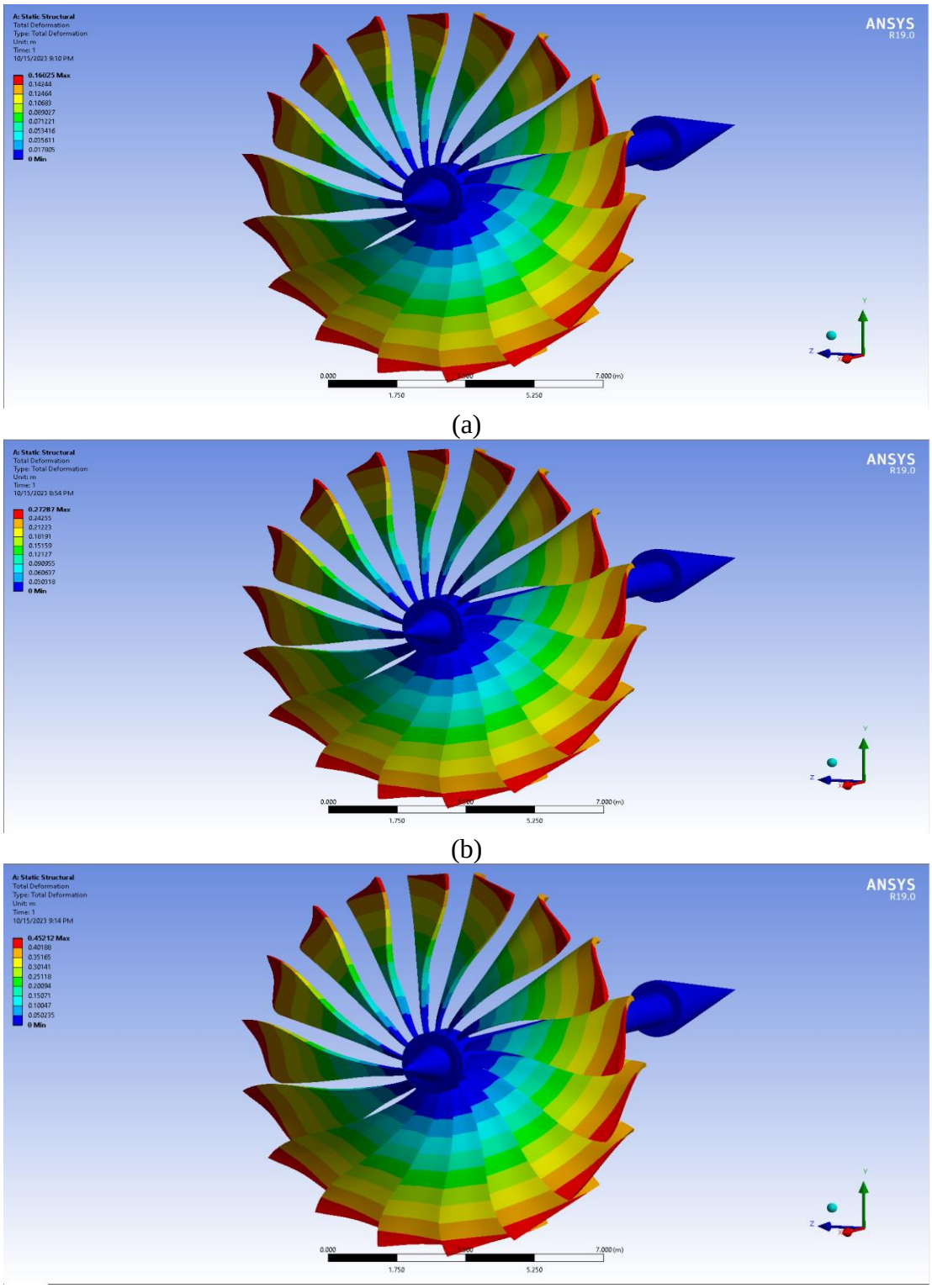

Figure 9. *Deformation contour at different speed. (a) 200 km/h, (b) 400 km/h, (c) 500 km/h.*

From Figure 10, which shows the stresses resulting from the force of the air on the turbine, it is noted that the value of the stresses reached 5.4 GPa at a speed of 600 km/h.

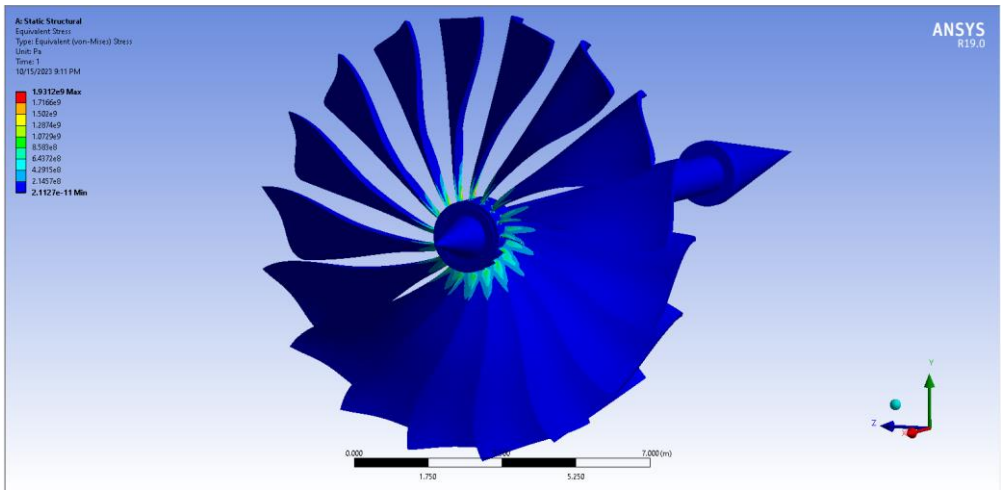

(a)

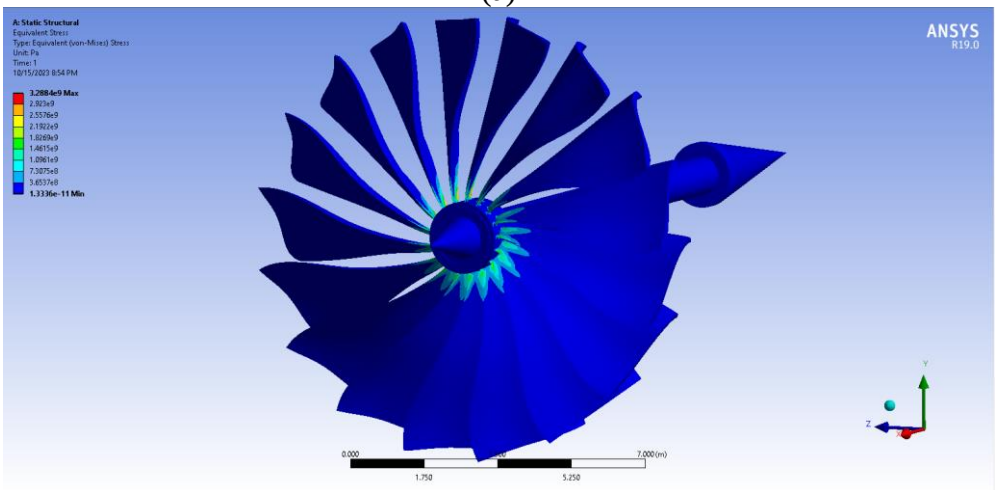

(b)

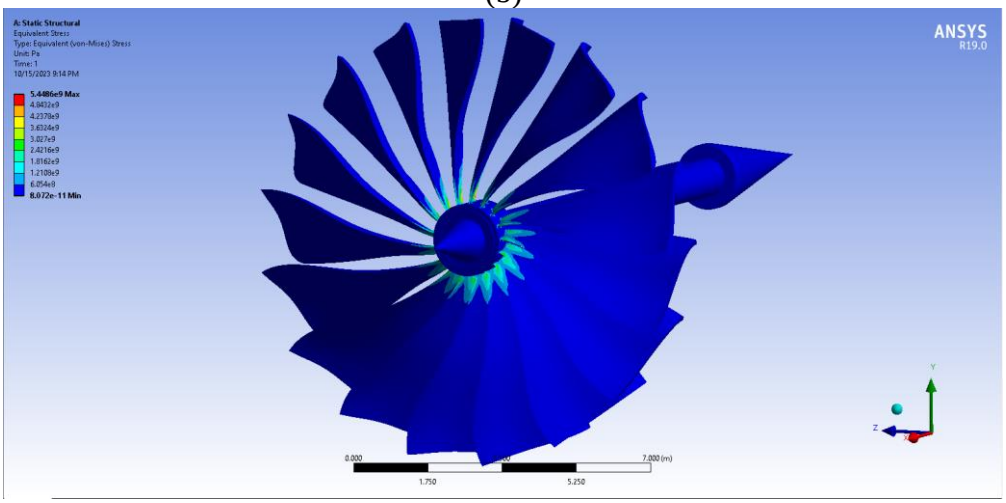

(c)

Figure 10. *Stress contour at different speed. (a) 200 km/h, (b) 400 km/h, (c) 500 km/h.*

4. Conclusions

The simulation of powder in aircraft engine turbine manufacturing involves creating a model of a standard engine and adding titanium powder layers to increase its aerodynamic resistance. The model is then entered into the FSI system, where aerodynamics are studied at

speeds of 200, 400, and 600 km/h. The properties of Ti–6Al–4V are then applied to the turbine structure using different thicknesses of powder.

1. The air flow speed and gradients of an engine turbine are influenced by the plane's speed, resulting in a force exerted on the turbine blades.
2. The thickness of the powder layer affects the amount of deformations caused by air force passing through turbine blades. The 5mm layer had the highest deformation at 0.73 m, while the 10mm and 15mm layers had the lowest at 0.44 m and 0.27 m respectively, indicating the benefits of powder technology.
3. The stress generated by the plane's force reached 3.2 GPa, while the deformation value reached 0.452 m at a speed of 600 km/h. The stress resulting from the air's force on the turbine reached 5.4 GPa at the same speed. The plane's speed also affected the formation of greater force and stress.

References

1. V.S. Telang, R. Pemmada, V. Thomas, S. Ramakrishna, P. Tandon, H.S. Nanda, Harnessing additive manufacturing for magnesium-based metallic bioimplants: Recent advances and future perspectives, Curr. Opin. Biomed. Eng. 17 (2021) 100264. https://doi.org/10.1016/j.cobme.2021.100264.
2. R. Allavikutty, P. Gupta, T.S. Santra, J. Rengaswamy, Additive manufacturing of Mg alloys for biomedical applications: Current status and challenges, Curr. Opin. Biomed. Eng. 18 (2021) 100276. https://doi.org/10.1016/j.cobme.2021.100276.
3. J.H. Kim, M.Y. Kim, J.C. Knowles, S. Choi, H. Kang, S. hyun Park, S.M. Park, H.W. Kim, J.T. Park, J.H. Lee, H.H. Lee, Mechanophysical and biological properties of a 3D-printed titanium alloy for dental applications, Dent. Mater. 36 (2020) 945–958. https://doi.org/10.1016/j.dental.2020.04.027.
4. L. Yang, C. Han, H. Wu, L. Hao, Q. Wei, C. Yan, Y. Shi, Insights into unit cell size effect on mechanical responses and energy absorption capability of titanium graded porous structures manufactured by laser powder bed fusion, J. Mech. Behav. Biomed. Mater. 109 (2020) 103843. https://doi.org/10.1016/j.jmbbm.2020.103843.
5. Y. Alshammari, M. Jia, F. Yang, L. Bolzoni, The effect of α+ β forging on the mechanical properties and microstructure of binary titanium alloys produced via a cost-effective powder metallurgy route, Mater. Sci. Eng. A. 769 (2020) 138496. https://doi.org/10.1016/j.msea.2019.138496.
6. M.M. Quazi, M. Ishak, M.A. Fazal, A. Arslan, S. Rubaiee, A. Qaban, M.H. Aiman, T. Sultan, M.M. Ali, S.M. Manladan, Current research and development status of dissimilar materials laser welding of titanium and its alloys, Opt. Laser Technol. 126 (2020) 106090. https://doi.org/10.1016/j.optlastec.2020.106090.
7. S.A. Smythe, B.M. Thomas, M. Jackson, Recycling of titanium alloy powders and swarf through continuous extrusion (Conformtm) into affordable wire for additive manufacturing, Metals (Basel). 10 (2020) 1–18. https://doi.org/10.3390/met10060843.
8. A.E. Davis, C.I. Breheny, J. Fellowes, U. Nwankpa, F. Martina, J. Ding, T. Machry, P.B. Prangnell, Mechanical performance and microstructural characterisation of titanium alloy-alloy composites built by wire-arc additive manufacture, Mater. Sci. Eng. A. 765 (2019) 138289. https://doi.org/10.1016/j.msea.2019.138289.
9. R. Subbarao, S. Chakraborty, Microscopic Studies on the Characteristics of Different Alloys Suitable for Gas Turbine Components, Mater. Today Proc. 5 (2018) 11576–11584. https://doi.org/10.1016/j.matpr.2018.02.126.
10. C.Y. Yap, C.K. Chua, Z.L. Dong, Z.H. Liu, D.Q. Zhang, L.E. Loh, S.L. Sing, Review of selective laser melting: Materials and applications, Appl. Phys. Rev. 2 (2015). https://doi.org/10.1063/1.4935926.

11. B. Song, S. Dong, H. Liao, C. Coddet, Process parameter selection for selective laser melting of Ti6Al4V based on temperature distribution simulation and experimental sintering, Int. J. Adv. Manuf. Technol. 61 (2012) 967–974. https://doi.org/10.1007/s00170-011-3776-6.
12. L.E. Murr, S.A. Quinones, S.M. Gaytan, M.I. Lopez, A. Rodela, E.Y. Martinez, D.H. Hernandez, E. Martinez, F. Medina, R.B. Wicker, Microstructure and mechanical behavior of Ti-6Al-4V produced by rapid-layer manufacturing, for biomedical applications, J. Mech. Behav. Biomed. Mater. 2 (2009) 20–32. https://doi.org/10.1016/j.jmbbm.2008.05.004.